polymers

MDPI

Article

Comparative X-ray Shielding Properties of Single-Layered and Multi-Layered Bi_2O_3/NR Composites: Simulation and Numerical Studies

Arkarapol Thumwong [1], Jitsuna Darachai [2] and Kiadtisak Saenboonruang [3,4,5,6,*]

1 Department of Materials Science, Faculty of Science, Kasetsart University, Bangkok 10900, Thailand; arkarapol.th@ku.th
2 Department of Engineering Physics, Tsinghua University, Beijing 100084, China; jitsuna.note@gmail.com
3 Department of Applied Radiation and Isotopes, Faculty of Science, Kasetsart University, Bangkok 10900, Thailand
4 Kasetsart Research and Development Institute, Kasetsart University, Bangkok 10900, Thailand
5 Specialized Center of Rubber and Polymer Materials in Agriculture and Industry (RPM), Faculty of Science, Kasetsart University, Bangkok 10900, Thailand
6 Special Research Unit of Radiation Technology for Advanced Materials, Faculty of Science, Kasetsart University, Bangkok 10900, Thailand
* Correspondence: kiadtisak.s@ku.th; Tel.: +66-2562-5555 (ext. 646219)

Abstract: This work theoretically compared the X-ray attenuation capabilities in natural rubber (NR) composites containing bismuth oxide (Bi_2O_3) by determining the effects of multi-layered structures on the shielding properties of the composites using two different software packages (XCOM and PHITS). The shielding properties of the single-layered and multi-layered Bi_2O_3/NR composites investigated consisted of the transmission factor (I/I_0), effective linear attenuation coefficient (μ_{eff}), effective mass attenuation coefficient ($\mu_{m,eff}$), and effective half-value layer (HVL_{eff}). The results, with good agreement between those obtained from XCOM and PHITS (with less than 5% differences), indicated that the three-layered NR composites (sample#4), with the layer arrangement of pristine NR (layer#1)-Bi_2O_3/NR (layer#2)-pristine NR (layer#3), had relatively higher X-ray shielding properties than either a single-layer or the other multi-layered structures for all X-ray energies investigated (50, 100, 150, and 200 keV) due to its relatively larger effective percentage by weight of Bi_2O_3 in the composites. Furthermore, by varying the Bi_2O_3 contents in the middle layer (layer#2) of sample#4 from 10 to 90 wt.%, the results revealed that the overall X-ray shielding properties of the NR composites were further enhanced with additional filler, as evidenced by the highest values of μ_{eff} and $\mu_{m,eff}$ and the lowest values of I/I_0 and HVL_{eff} observed in the 90 wt.% Bi_2O_3/NR composites. In addition, the recommended Bi_2O_3 contents for the actual production of three-layered Bi_2O_3/NR composites (the same layer structure as sample#4) were determined by finding the least Bi_2O_3 content that enabled the sample to attenuate incident X-rays with equal efficiency to that of a 0.5-mm lead sheet (with an effective lead equivalence of 0.5 mmPb). The results suggested that the recommended Bi_2O_3 contents in layer#2 were 82, 72, and 64 wt.% for the combined 6 mm, 9 mm, and 12 mm samples, respectively.

Keywords: natural rubber; Bi_2O_3; X-ray shielding; simulation; multi-layered structure

check for updates

Citation: Thumwong, A.; Darachai, J.; Saenboonruang, K. Comparative X-ray Shielding Properties of Single-Layered and Multi-Layered Bi_2O_3/NR Composites: Simulation and Numerical Studies. *Polymers* **2022**, *14*, 1788. https://doi.org/10.3390/polym14091788

Academic Editors: Albertino Arteiro and Mohammad Arjmand

Received: 25 March 2022
Accepted: 26 April 2022
Published: 27 April 2022

1. Introduction

Since the discovery of X-rays in 1895 by Wilhelm Roentgen, various applications have relied heavily on the utilization of X-ray technologies, especially X-ray imaging and X-ray irradiation in medicine, industry, material characterization, security, the arts, foods, and agriculture [1–6]. Despite their great potential and usefulness, excessive exposure to X-rays could harmfully affect the health of users and the public, with various symptoms, including nausea, skin burn, diarrhea, permanent disability, cancer, and death, depending on the exposure dose and duration as well as the sex, health condition, and age of those exposed [7,8]. Hence, to reduce and/or prevent the risks of excessive exposure to X-rays, a radiation safety principle, namely "As Low As Reasonably Achievable" or "ALARA", must be strictly followed in all nuclear facilities to ensure the safety of all users and the public [9].

One of the three safety measures in ALARA is the utilization of sufficient and appropriate shielding equipment; for which different applications may require different types and specific properties from the materials [10]. For example, X-ray shielding materials based on polyethylene (PE), including Gd_2O_3/HDPE and nano-ZnO/HDPE composites, are suitable for applications that require exceptional strength and rigidity, such as those involving products for use as movable panels, walls, and construction parts in nuclear facilities [11,12]. On the other hand, shielding equipment, such as personal protective equipment (PPE) and covers for transporting casks, requiring exceptional flexibility, high strength, and a large amount of elongation from the materials, relies on natural and synthetic rubber composites. For example, Bi_2O_3/NR, Bi_2O_3/EPDM, $BaSO_4$/EPDM, and W/SR composites were among recently developed X-ray shielding rubber materials that offered not only effective X-ray attenuation abilities but also sufficient mechanical strength and flexibility to the users [13–16]. Notably, these mentioned examples of X-ray shielding materials are lead-free, which is presently sought-after in materials, as they could substantially reduce the risks to users from exposure to highly toxic lead (Pb) elements and compounds that are common protective fillers used for the manufacturing of X-ray and gamma shielding materials due to their economical accessibility and excellent attenuation capability [17,18].

Generally, the addition of heavy metals, including Bi_2O_3, to the main matrix is a common method to enhance the X-ray attenuation abilities of the composites, mainly due to the relatively high atomic number (Z) and density (ρ) of Bi_2O_3 that enhance the interaction probabilities between the incident X-rays and the materials, subsequently increasing the ability to attenuate the incident X-rays of the composites [19]. Some examples showing the effects of Bi_2O_3 on improving the shielding capabilities of the composites have been reported by Intom et al., who showed that the mass attenuation coefficients (μ_m) of Bi_2O_3/NR composites increased from 0.1324 to 0.3847 and then to 0.4779 cm^2/g when the Bi_2O_3 contents in the NR composites increased from 0 to 80 and then to 150 parts per hundred parts of rubber by weight (phr), respectively (determined at an energy level of 223 keV) [20]. Similarly, the report from Toyen et al. suggested that increases in the Bi_2O_3 contents from 0 to 300 and then to 500 phr increased the linear attenuation coefficients (μ) of NR composites from 2.1 to 14.7 and then to 20.4 m^{-1}, respectively (determined at an energy level of 662 keV) [13].

Nonetheless, despite the positive relationship between the contents of Bi_2O_3 and the shielding properties of the composites, increases in Bi_2O_3 contents may lead to undesirable reductions in the mechanical properties, such as decreased values of the tensile strength and elongation at the break of Bi_2O_3/NR composites from 14 to 7 MPa and from 630% to 500%, respectively, when the Bi_2O_3 contents increase from 100 to 500 phr [13]. This behavior was observed mainly due to particle agglomerations caused by filler–filler interactions and phase separation at higher filler contents [14,21]. To alleviate or limit such drawbacks by adding high filler contents to the composites, one possible method is to prepare the materials with multi-layered structures, which would enable the pristine NR layers to better support and transfer external forces exerted on the Bi_2O_3/NR layers, consequently limiting the reduction in the overall strength of the materials [22,23].

As aforementioned, due to the competing roles of Bi_2O_3 in the enhancement of X-ray-shielding properties and the reductions in mechanical properties, this work investigated appropriate multi-layered structures of Bi_2O_3/NR composites by theoretically comparing X-ray shielding parameters, consisting of the transmission factor (I/I_0), the effective mass attenuation coefficient (μ_{eff}), the effective linear attenuation coefficient ($\mu_{m,eff}$), the effective half-value layer (HVL_{eff}), and the effective lead equivalence ($Pb_{eq,eff}$), from 11 distinct multi-layered structures using XCOM and PHITS. In addition, the recommended Bi_2O_3 contents for the multi-layered structure that produced the highest shielding properties were also determined by finding the least Bi_2O_3 contents that, when being added to the NR composites, produced the required $Pb_{eq,eff}$ value of 0.5 mmPb. The outcomes of this work would not only provide comparative X-ray shielding properties of multi-layered products but also present promising methods to preserve the mechanical properties of shielding materials containing high contents of fillers.

2. Determination of X-ray Shielding Properties Using XCOM and PHITS

2.1. Multi-Layered Structures of Bi_2O_3/NR Composites

The details and schemes of 11 distinct multi-layered structures for Bi_2O_3/NR composites with varying numbers (1–5) of layers and varying Bi_2O_3 contents for each layer are shown in Table 1 and Figure 1, respectively. In order to simplify the setups for the determination of X-ray shielding properties, all samples would have the same average weight contents per thickness, i.e., $\Sigma C_i x_i / \Sigma x_i$ where C_i and x_i are Bi_2O_3 content and thickness of the ith layer, respectively. Notably, for Figure 1, the left surface of each design was the side that faced the incident X-rays.

Table 1. Sample codes with details of the number of layers, thickness of each layer, and Bi_2O_3 content in each layer for determination of X-ray shielding properties in Bi_2O_3/NR composites (Sample# and Layer# denote Sample Number and Layer Number, respectively).

Sample#	Number of Layers	Thickness of Each Layer (mm)	Bi_2O_3 Contents in Layer# (wt.%)				
			1	2	3	4	5
1	1	6.0	10	-	-	-	-
2	2	3.0	0	20	-	-	-
3	2	3.0	20	0	-	-	-
4	3	2.0	0	30	0	-	-
5	3	2.0	15	0	15	-	-
6	4	1.5	20	0	20	0	-
7	4	1.5	0	20	0	20	-
8	4	1.5	0	20	20	0	-
9	4	1.5	20	0	0	20	-
10	5	1.2	16.7	0	16.7	0	16.7
11	5	1.2	0	25	0	25	0

2.2. Determination of X-ray Shielding Properties Using XCOM

The X-ray shielding properties of all 11 multi-layered structures at the X-ray energies of 50, 100, 150, and 200 keV were numerically determined using the web-based XCOM software, provided by the National Institute of Standards and Technology (NIST) (Gaithersburg, MD, USA) [24,25]. The NIST standard reference database 8 (XGAM), released in 2010, was used as the photon cross-section database in this work and the X-ray shielding parameters were calculated from the total attenuation with the inclusion of coherent scattering [26].

In order to obtain the final transmission factor (I/I_0) for each design, the mass attenuation coefficient (μ_m) for the Bi_2O_3/NR composites containing varying Bi_2O_3 contents of 0, 10, 15, 16.7, 20, 25, and 30 wt.% were determined using XCOM. The details of the procedure to input material parameters and contents have been described elsewhere [24]. Then, the linear attenuation coefficients (μ) for each corresponding Bi_2O_3 content were determined using the obtained μ_m, following Equation (1):

$$\mu = \mu_m \times \rho \tag{1}$$

where ρ is the density of the Bi_2O_3/NR composites containing varying Bi_2O_3 contents of 0, 10, 15, 16.7, 20, 25, and 30 wt.%, theoretically calculated using Equation (2):

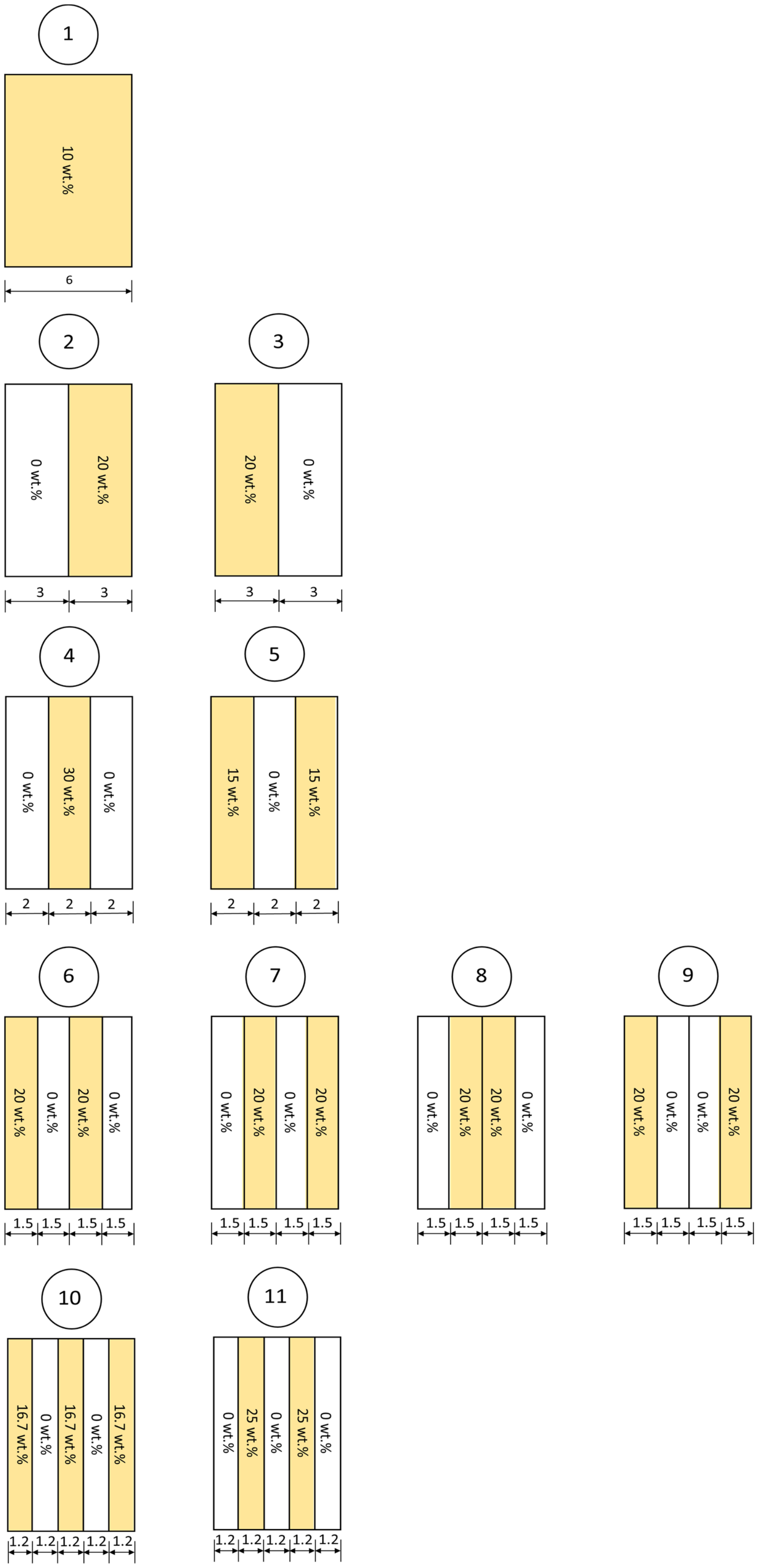

Figure 1. Schemes showing single-layered and multi-layered structures and Bi_2O_3 contents for 11 distinct designs for determination of X-ray shielding properties in Bi_2O_3/NR composites, where thicknesses are in millimeters and the numbers enclosed in circles represent the sample#.

$$\rho = \frac{100}{\frac{C_{NR}}{\rho_{NR}} + \frac{C_{Bi_2O_3}}{\rho_{Bi_2O_3}}} \quad (2)$$

where ρ_{NR} ($\rho_{Bi_2O_3}$) is the density of NR (Bi_2O_3), which is 0.92 g/cm^3 (8.90 g/cm^3), and C_{NR} ($C_{Bi_2O_3}$) is the weight content of NR (Bi_2O_3) in the composites. Notably, $C_{NR} + C_{Bi_2O_3}$ = 100 wt.%.

The value of $(I/I_0)_i$ for the ith layer was calculated from its corresponding μ using Equation (3):

$$\left(\frac{I}{I_0}\right)_i = e^{-\mu x_i} \quad (3)$$

where x_i is the thickness of the ith layer for each design shown in Table 1. Then, the final I/I_0 value for each sample was calculated by multiplying individual $(I/I_0)_i$ values from each layer, according to Equation (4):

$$\frac{I}{I_0} = \prod\nolimits_1^n \left(\frac{I}{I_0}\right)_i \quad (4)$$

where n is the number of layers in the sample and i is 1, 2, . . . , n.

Lastly, the effective linear attenuation coefficient (μ_{eff}), the effective mass attenuation coefficient ($\mu_{m,eff}$), and the effective half-value layer (HVL_{eff}), which represented the overall X-ray shielding properties for each design, were determined using Equations (5)–(7), respectively:

$$\mu_{eff} = \frac{-\ln\left(\frac{I}{I_0}\right)_i}{x_i} \quad (5)$$

$$\mu_{m,eff} = \frac{\mu_{eff}}{\rho_{eff}} \quad (6)$$

$$HVL_{eff} = \frac{\ln(2)}{\mu_{eff}} \quad (7)$$

where ρ_{eff} is the effective density of the sample, calculated using Equation (8):

$$\rho_{eff} = \frac{\sum_1^n \rho_i x_i}{\sum_1^n x_i} \quad (8)$$

where ρ_i and x_i are the density and the thickness of the ith layer, respectively. Notably, for further determination, the values of μ for a pure Pb sheet at X-ray energies of 50, 100, 150, and 200 keV were also determined using XCOM. Furthermore, the effective percentage by weight (C_{eff,Bi_2O_3}) of Bi_2O_3 in different multi-layered samples (sample#2–sample#11) was also determined using Equation (9), which was derived from Equation (2):

$$\rho_{eff} = \frac{100}{\frac{100-C_{eff,Bi_2O_3}}{\rho_{NR}} + \frac{C_{eff,Bi_2O_3}}{\rho_{Bi_2O_3}}} \quad (9)$$

2.3. Determination of X-ray Shielding Properties Using PHITS

In order to verify the X-ray shielding properties obtained using XCOM, the final I/I_0 values were also determined for all multi-layered structures using PHITS by setting up the incident X-ray beam with a diameter of 1 mm pointing directly to the center of each sample, having a surface area of 20 cm × 20 cm and a combined thickness of 6 mm. This setup would minimize the possible overestimation of the final I/I_0 value caused by build-up effects [27]. In addition, the detector with a 100% detection efficiency was set up to capture all primary transmitted X-rays. Further details of the PHITS setup are provided elsewhere [10,11]. The percentages of difference (%Difference) between the final I/I_0 values obtained from XCOM and those from PHITS were determined, following Equation (10):

$$\%\text{Difference} = \frac{\left|\left(\frac{I}{I_0}\right)_{\text{XCOM}} - \left(\frac{I}{I_0}\right)_{\text{PHITS}}\right|}{\left(\frac{I}{I_0}\right)_{\text{XCOM}}} \times 100\% \tag{10}$$

where $(I/I_0)_{XCOM}$ and $(I/I_0)_{PHITS}$ are the effective transmission factors of the Bi_2O_3/NR composites obtained from XCOM and PHITS, respectively.

2.4. Determination of Effective Lead Equivalence and Recommended Contents of Bi_2O_3

The values of effective lead equivalence ($Pb_{eq,eff}$) at X-ray energies of 50, 100, 150, and 200 keV for the multi-layered Bi_2O_3/NR composites offering the highest final I/I_0 values among all 11 designs were calculated, following Equation (11):

$$\mu_{Pb} Pb_{eq,eff} = \mu_{NR,eff} x_{NR} \tag{11}$$

where μ_{Pb} is the linear attenuation coefficient of a pure Pb sheet, $\mu_{NR,eff}$ is the effective linear attenuation coefficient of multi-layered Bi_2O_3/NR composites, and x_{NR} is the combined thickness of the multi-layered Bi_2O_3/NR composites, which varied from 6 to 9 to 12 mm. Notably, the Bi_2O_3 contents for the determination of $Pb_{eq,eff}$ were varied up to the maximum content of 90 wt.% and the μ_{Pb} values were 90.9, 62.7, 22.8, and 1.13 cm^{-1} at X-ray energies of 50, 100, 150, and 200 keV, respectively, determined using XCOM.

To determine the recommended Bi_2O_3 contents, the values of $Pb_{eq,eff}$ for all conditions obtained from the previous steps were plotted against their corresponding Bi_2O_3 contents. Then, a horizontal straight line with a Pb_{eq} value of 0.5 mmPb (the common requirement for X-ray shielding equipment in general nuclear facilities) was plotted and the points of intersection were noted for each thickness (6, 9, and 12 mm), which represented the least Bi_2O_3 contents providing the composites with a Pb_{eq} value of 0.5 mmPb, and could be regarded as the recommended Bi_2O_3 contents for the actual production.

3. Results and Discussion

3.1. Values of μ_m, μ, and ρ for Bi_2O_3/NR Composites

The values of the numerically determined μ_m, ρ, and μ for the single-layered Bi_2O_3/NR composites with varying Bi_2O_3 contents of 0, 10, 15, 16.7, 20, 25, or 30 wt.% at X-ray energies of 50, 100, 150, and 200 keV are shown in Tables 2–4, respectively. The results shown in Table 2 indicated that the values of μ_m tended to increase with increasing Bi_2O_3 content but decreased with increasing X-ray energy. The positive relationship between μ_m and filler contents was mainly due to the high atomic number (Z) of Bi and the much higher density (ρ) of Bi_2O_3 compared to those of NR, resulting in substantially enhanced interaction probabilities between the incident X-rays and the materials through the very effective and dominant X-ray interaction, namely photoelectric absorption, which subsequently improved the overall X-ray shielding properties of the composites with the addition of Bi_2O_3. The behavior could be mathematically explained by considering the relationship between the photoelectric cross-section (σ_{pe}), atomic numbers (Z) of elements in the composites, and the frequencies (ν) of incident X-rays, following Equation (12):

$$\sigma_{pe} = \frac{Z^n}{(h\nu)^3} \tag{12}$$

where h is Planck's constant [11].

Table 2. Mass attenuation coefficients (μ_m; cm^2/g) of Bi_2O_3/NR composites with varying Bi_2O_3 contents of 0, 10, 15, 16.7, 20, 25, and 30 wt.% at the X-ray energies of 50, 100, 150, and 200 keV.

X-ray Energy (keV)	Bi_2O_3 Content (wt.%)						
	0	**10**	**15**	**16.7**	**20**	**25**	**30**
50	0.2047	0.9379	1.3050	1.4290	1.6710	2.0380	2.4040
100	0.1683	0.6677	0.9174	1.0020	1.1670	1.4170	1.6670
150	0.1501	0.3233	0.4099	0.4393	0.4965	0.5831	0.6696
200	0.1371	0.2174	0.2575	0.2712	0.2976	0.3378	0.3779

Table 3. Calculated densities (ρ) of Bi_2O_3/NR composites with varying Bi_2O_3 contents of 0, 10, 15, 16.7, 20, 25, and 30 wt.%.

Bi_2O_3 Content (wt.%)	Density (g/cm^3)
0	0.920
10	1.011
15	1.063
16.7	1.082
20	1.121
25	1.186
30	1.259

Table 4. Linear attenuation coefficients (μ; cm^{-1}) of single-layered Bi_2O_3/NR composites with varying Bi_2O_3 contents of 0, 10, 15, 16.7, 20, 25, and 30 wt.% at X-ray energies of 50, 100, 150, and 200 keV.

X-ray Energy (keV)	Bi_2O_3 Content (wt.%)						
	0	**10**	**15**	**16.7**	**20**	**25**	**30**
50	0.1883	0.9478	1.3872	1.5457	1.8732	2.4167	3.0255
100	0.1548	0.6747	0.9751	1.0838	1.3082	1.6803	2.0979
150	0.1380	0.3267	0.4357	0.4751	0.5565	0.6914	0.8427
200	0.1261	0.2197	0.2737	0.2933	0.3336	0.4005	0.4755

Notably, ν and the X-ray energy (E) are directly proportional to each other as shown in Equation (13):

$$E = h\nu \quad (13)$$

Equations (12) and (13) also depict that the interaction probabilities between the incident X-rays and the materials are inversely proportional to ν^3 or E^3; for which the results in Table 2 clearly illustrate this effect, as evidenced by the lowest μ_m values being observed at the X-ray energy of 200 keV [28].

Table 3, which shows the calculated densities (ρ) of a single-layered Bi_2O_3/NR composite with varying Bi_2O_3 contents of 0, 10, 15, 16.7, 20, 25, and 30 wt.% that were used for the determination of the linear attenuation coefficient (μ), suggested that the density of the NR composites increased with increasing Bi_2O_3 contents, which is mainly due to the much higher ρ value of Bi_2O_3 ($\rho_{Bi_2O_3}$ = 8.90 g/cm^3) than for NR (ρ_{NR} = 0.92 g/cm^3). Using the results shown in Tables 2 and 3, and Equation (1), the values of μ for all the single-layered Bi_2O_3/NR composites with varying Bi_2O_3 contents of 0, 10, 15, 16.7, 20, 25, and 30 wt.% were determined, and the results are shown in Table 4, which indicates similar behavior as for μ_m (Table 2). However, more pronounced effects of Bi_2O_3 on the enhancement of μ were observed compared to those for μ_m due to the simultaneous roles of Bi_2O_3 in increasing both the μ_m and ρ values of the composites, which further amplified the values of μ at higher Bi_2O_3 contents (Equation (1)).

3.2. Final I/I_0 of Multi-Layered Bi_2O_3/NR Composites

Tables 5–8 show the transmission factors (I/I_0) for each layer as well as the final I/I_0 values of the 11 multi-layered Bi_2O_3/NR composites at X-ray energies of 50, 100, 150, and 200 keV, respectively, and Figure 2 shows the schematic representation of relative X-ray intensities for each layer of some designs at the X-ray energy of 50 keV. All the results suggested that the NR layers containing Bi_2O_3 could attenuate X-rays with higher efficiencies than those without Bi_2O_3 due to the much higher μ values of Bi_2O_3/NR composites (Table 4), especially those with higher Bi_2O_3 contents, that better interacted and attenuated incident X-rays. Furthermore, the results revealed that the final I/I_0 values for the composites had larger transmitted X-ray intensities at higher X-ray energies (for the same sample#). This behavior could be explained using Equation (12), which suggested that the interaction probabilities, as well as their X-ray attenuation capabilities, decreased with increasing X-ray energies, resulting in more X-rays being able to escape the materials.

Table 5. Relative X-ray intensities for each layer of multi-layered Bi_2O_3/NR composites at an X-ray energy of 50 keV (Sample# and Layer# denote Sample Number and Layer Number, respectively).

Sample#	Number of Layers	Thickness of Each Layer (mm)	Relative X-ray Intensities for Layer#				
			1	2	3	4	5
1	1	6.0	0.5663	-	-	-	-
2	2	3.0	0.9451	0.5388	-	-	-
3	2	3.0	0.5701	0.5388	-	-	-
4	3	2.0	0.9630	0.5258	0.5064	-	-
5	3	2.0	0.7577	0.7298	0.5529	-	-
6	4	1.5	0.7550	0.7340	0.5542	0.5388	-
7	4	1.5	0.9722	0.7340	0.7136	0.5388	-
8	4	1.5	0.9722	0.7340	0.5542	0.5388	-
9	4	1.5	0.7550	0.7340	0.7136	0.5388	-
10	5	1.2	0.8307	0.8121	0.6746	0.6596	0.5479
11	5	1.2	0.9777	0.7315	0.7152	0.5352	0.5232

Table 6. Relative X-ray intensities for each layer of multi-layered Bi_2O_3/NR composites at an X-ray energy of 100 keV (Sample# and Layer# denote Sample Number and Layer Number, respectively).

Sample#	Number of Layers	Thickness of Each Layer (mm)	Relative X-ray Intensities for Layer#				
			1	2	3	4	5
1	1	6.0	0.6671	-	-	-	-
2	2	3.0	0.9546	0.6447	-	-	-
3	2	3.0	0.6754	0.6447	-	-	-
4	3	2.0	0.9695	0.6373	0.6178	-	-
5	3	2.0	0.8228	0.7977	0.6564	-	-
6	4	1.5	0.8218	0.8030	0.6599	0.6447	-
7	4	1.5	0.9770	0.8030	0.7845	0.6447	-
8	4	1.5	0.9770	0.8030	0.6599	0.6447	-
9	4	1.5	0.8218	0.8030	0.7845	0.6447	-
10	5	1.2	0.8780	0.8619	0.7568	0.7428	0.6522
11	5	1.2	0.9816	0.8023	0.7876	0.6438	0.6319

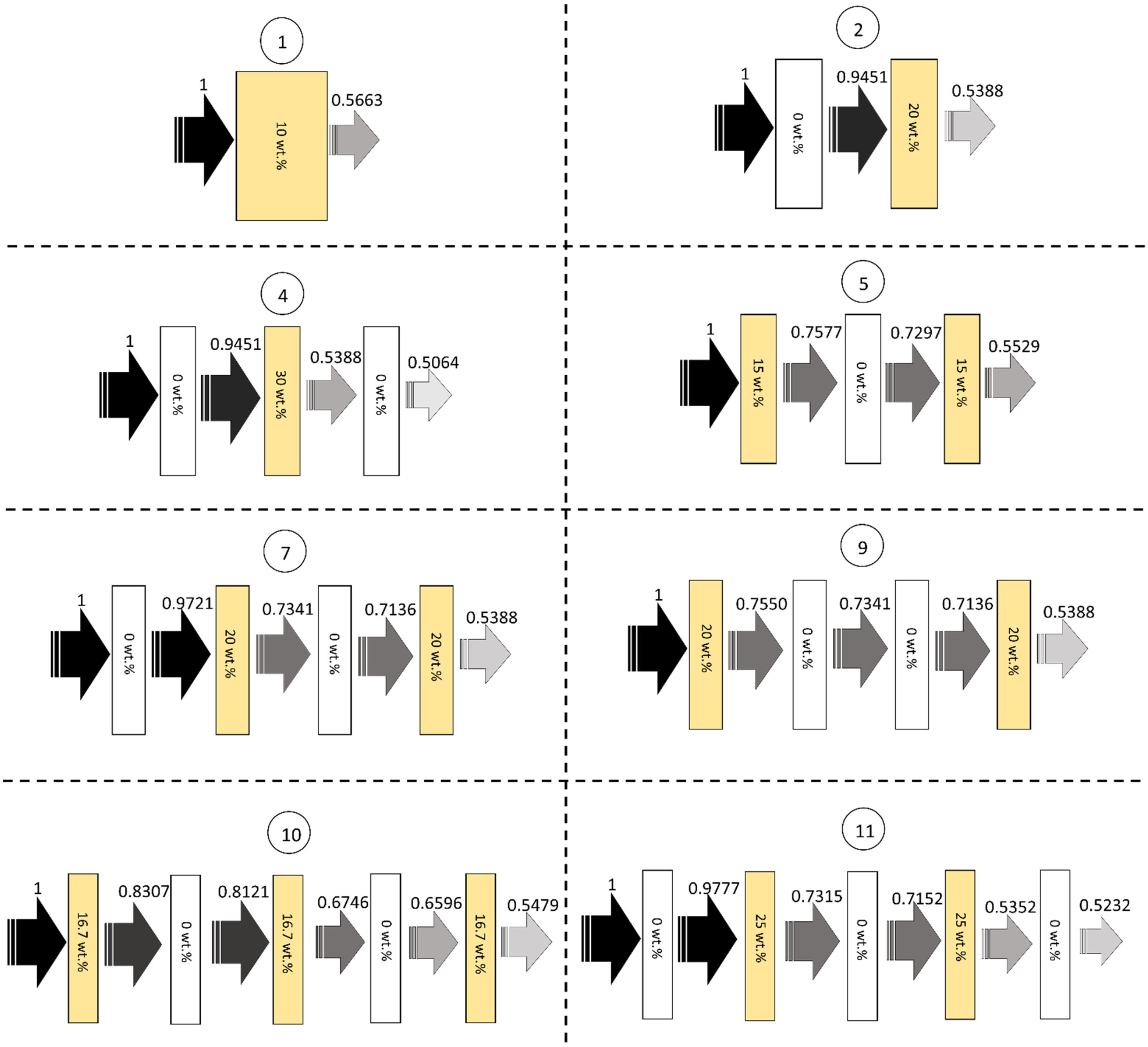

Figure 2. Schemes showing relative X-ray intensities for each layer of sample#1, sample#2, sample#4, sample#5, sample#7, sample#9, sample#10, and sample#11, at the X-ray energy of 50 keV. The numbers enclosed in circles represent sample#.

Table 7. Relative X-ray intensities for each layer of multi-layered Bi_2O_3/NR composites at an X-ray energy of 150 keV (Sample# and Layer# denote Sample Number and Layer Number, respectively).

Sample#	Number of Layers	Thickness of Each Layer (mm)	Relative X-ray Intensities for Layer#				
			1	2	3	4	5
1	1	6.0	0.8220	-	-	-	-
2	2	3.0	0.9594	0.8119	-	-	-
3	2	3.0	0.8462	0.8119	-	-	-
4	3	2.0	0.9728	0.8219	0.7995	-	-
5	3	2.0	0.9165	0.8916	0.8172	-	-
6	4	1.5	0.9199	0.9010	0.8289	0.8119	-
7	4	1.5	0.9795	0.9010	0.8826	0.8119	-
8	4	1.5	0.9795	0.9010	0.8289	0.8119	-
9	4	1.5	0.9199	0.9010	0.8826	0.8119	-
10	5	1.2	0.9446	0.9291	0.8776	0.8631	0.8153
11	5	1.2	0.9836	0.9052	0.8904	0.8195	0.8060

Table 8. Relative X-ray intensities for each layer of multi-layered Bi_2O_3/NR composites at an X-ray energy of 200 keV (Sample# and Layer# denote Sample Number and Layer Number, respectively).

Sample#	Number of Layers	Thickness of Each Layer (mm)	Relative X-ray intensities for Layer#				
			1	2	3	4	5
1	1	6.0	0.8765	-	-	-	-
2	2	3.0	0.9629	0.8712	-	-	-
3	2	3.0	0.9048	0.8712	-	-	-
4	3	2.0	0.9751	0.8866	0.8645	-	-
5	3	2.0	0.9467	0.9231	0.8740	-	-
6	4	1.5	0.9512	0.9334	0.8878	0.8712	-
7	4	1.5	0.9813	0.9334	0.9159	0.8712	-
8	4	1.5	0.9813	0.9334	0.8878	0.8712	-
9	4	1.5	0.9512	0.9334	0.9159	0.8712	-
10	5	1.2	0.9654	0.9509	0.9180	0.9042	0.8729
11	5	1.2	0.9850	0.9388	0.9247	0.8813	0.8680

Among the 11 multi-layered designs, sample#4, which has a three-layered structure, had the lowest final I/I_0 values of 0.5064, 0.6178, 0.7995, and 0.8645 at X-ray energies of 50, 100, 150, and 200 keV, respectively, while sample#1, a single-layered structure, had the highest final I/I_0 values of 0.5663, 0.6671, 0.8220, and 0.8765 at X-ray energies of 50, 100, 150, and 200 keV, respectively. Based on the results from these two designs, the multi-layered structure exhibited higher X-ray shielding capabilities by as much as 10.5, 8.7, 4.0, and 2.1% compared to a single-layered structure, determined at X-ray energies of 50, 100, 150, and 200 keV, respectively. Specifically, for sample#4, its highest X-ray attenuation capability was due to its highest effective density and effective percentage by weight of Bi_2O_3 contained in the sample, determined using Equations (8) and (9); for which the results of both parameters for all designs are shown in Table 9. The larger values of both quantities in multi-layered structures were mainly due to the much higher density of Bi_2O_3 particles in comparison with that of the NR matrix (for instance, adding 20 wt.% of Bi_2O_3 to layer#2 in sample#4 would require much less volume than removing 20 wt.% of NR, resulting in a considerable reduction in the total volume and subsequently the increase in the density of the sample). These effects then enabled sample#4 to have more Bi atoms to interact with incoming X-rays through the photoelectric absorption than that of sample#1.

Table 9. Effective densities and effective percentages by weight of Bi_2O_3 for all 11 multi-layered Bi_2O_3/NR composites (Sample# denotes Sample Number).

Sample#	Effective Density (g/cm^3)	Effective Percentage by Weight (wt.%)
1	1.011	10.00
2	1.021	10.98
3	1.021	10.98
4	1.033	12.19
5	1.015	10.47
6	1.021	10.98
7	1.021	10.98
8	1.021	10.98
9	1.021	10.98
10	1.017	10.64
11	1.026	11.55

In addition, Equation (3) could be modified for the calculation of I/I_0 as Equation (14):

$$\frac{I}{I_0} = e^{-\sum_i^N \mu_i x_i} \tag{14}$$

where μ_i is the linear attenuation coefficient of the ith layer, x_i is the thickness of the ith layer, and N is the total number of layers in the composites [29], which depicted that the values of $\sum_i^N \mu_i x_i$ for the multi-layered structures (using information from Tables 1 and 4) were larger than that of the single-layered sample. For instance, sample#4 had the value of $\sum_i^N \mu_i x_i$ of 0.6804, while sample#1 had the value of 0.5687, leading to a lower I/I_0 and better X-ray shielding capabilities in sample#4. Furthermore, the results showed that rearranging layers of the samples having the same Bi_2O_3 contents and numbers of layers did not have effects on X-ray shielding capabilities. For instance, sample #2 and sample #3, as well as samples #6–#9, had the same values of I/I_0, regardless of how the layers were arranged. This was due to the values of $\sum_i^N \mu_i x_i$ being the same for all of them.

Table 10 shows the final I/I_0 values of all 11 multi-layered structures using XCOM and PHITS, as well as their corresponding %Difference values for these two methods. The comparisons indicated that the results obtained from both methods were in good agreement, with the largest %Difference value being 4.78% and the average %Difference being 2.24%. Consequently, the values obtained from XCOM and PHITS could be further used for the determination of other parameters, including $\mu_{m,eff}$, μ_{eff}, HVL_{eff}, and $Pb_{eq,eff}$. Another interesting outcome from Table 9 was that the final I/I_0 values from PHITS seemed to be slightly higher than those from XCOM. This could have been due to factors, such as backscattering and the rescattering of X-rays inside the materials, resulting in an increase in the transmitted X-rays and a subsequent underestimation of the theoretical or ideal X-ray attenuation capabilities of the composites in the results obtained from PHITS [30].

Table 10. Comparative final transmission factors (I/I_0) of 11 multi-layered structures of Bi_2O_3/NR composites at X-ray energies of 50, 100, 150, and 200 keV using XCOM and PHITS and their corresponding percentage differences (Sample# denotes Sample Number).

Sample#	XCOM				PHITS				%Difference			
	Final Transmission Factor (I/I_0) at X-ray Energy (keV)											
	50	100	150	200	50	100	150	200	50	100	150	200
1	0.5663	0.6671	0.8220	0.8765	0.5732	0.6681	0.8258	0.8785	1.22	0.15	0.46	0.23
2	0.5388	0.6447	0.8119	0.8712	0.5518	0.6483	0.8498	0.8964	2.42	0.55	4.67	2.89
3	0.5388	0.6447	0.8119	0.8712	0.5578	0.6756	0.8196	0.8946	3.54	4.78	0.95	2.69
4	0.5064	0.6178	0.7995	0.8645	0.5289	0.6371	0.8255	0.8865	4.44	3.11	3.25	2.54
5	0.5529	0.6564	0.8172	0.8740	0.5766	0.6589	0.8443	0.8871	4.27	0.38	3.32	1.50
6	0.5388	0.6447	0.8119	0.8712	0.5428	0.6480	0.8226	0.8735	0.75	0.50	1.32	0.27
7	0.5388	0.6447	0.8119	0.8712	0.5494	0.6547	0.8432	0.8898	1.97	1.54	3.85	2.14
8	0.5388	0.6447	0.8119	0.8712	0.5471	0.6452	0.8461	0.8917	1.55	0.08	4.22	2.36
9	0.5388	0.6447	0.8119	0.8712	0.5596	0.6522	0.8480	0.8789	3.87	1.15	4.45	0.89
10	0.5479	0.6522	0.8153	0.8729	0.5550	0.6723	0.8523	0.8861	1.30	3.08	4.54	1.50
11	0.5232	0.6319	0.8060	0.8680	0.5297	0.6384	0.8343	0.9039	1.24	1.03	3.51	4.13

3.3. Values for μ_{eff}, $\mu_{m,eff}$, and HVL_{eff} of Multi-Layered Bi_2O_3/NR Composites

Table 11 shows the values of μ_{eff}, $\mu_{m,eff}$, and HVL_{eff} for the 11 multi-layered Bi_2O_3/NR composites at X-ray energies of 50, 100, 150, and 200 keV, determined using Equations (5)–(7) and the effective densities (ρ_{eff}) of the samples shown in Table 9. The results indicated that similar to those of the final I/I_0 (Table 10), sample#4 had the most efficient X-ray shielding properties as well as ρ_{eff}, as evidenced by its highest values of μ_{eff}, $\mu_{m,eff}$, and HVL_{eff} compared to the other designs.

Table 11. Values for μ_{eff}, $\mu_{m,eff}$, and HVL_{eff} of 11 multi-layered Bi_2O_3/NR composites at X-ray energies of 50, 100, 150, and 200 keV (Sample# denotes Sample Number).

Sample#	μ_{eff} (cm^{-1})				$\mu_{m,eff}$ (cm^2/g)				HVL_{eff} (cm)			
	50 keV	100 keV	150 keV	200 keV	50 keV	100 keV	150 keV	200 keV	50 keV	100 keV	150 keV	200 keV
1	0.9479	0.6748	0.3267	0.2197	0.9379	0.7195	0.4541	0.4838	0.7313	1.0272	2.1215	3.1549
2	1.0308	0.7315	0.3473	0.2299	1.0101	0.7243	0.4796	0.4793	0.6724	0.9475	1.9956	3.0153
3	1.0308	0.7315	0.3473	0.2299	1.0101	0.7243	0.4796	0.4793	0.6724	0.9475	1.9956	3.0153
4	1.1341	0.8025	0.3730	0.2426	1.0980	0.7309	0.5103	0.4755	0.6112	0.8637	1.8585	2.8569
5	0.9876	0.7017	0.3365	0.2245	0.9727	0.7214	0.4664	0.4814	0.7019	0.9878	2.0599	3.0873
6	1.0308	0.7315	0.3473	0.2299	1.0101	0.7243	0.4796	0.4793	0.6724	0.9475	1.9956	3.0153
7	1.0308	0.7315	0.3473	0.2299	1.0101	0.7243	0.4796	0.4793	0.6724	0.9475	1.9956	3.0153
8	1.0308	0.7315	0.3473	0.2299	1.0101	0.7243	0.4796	0.4793	0.6724	0.9475	1.9956	3.0153
9	1.0308	0.7315	0.3473	0.2299	1.0101	0.7243	0.4796	0.4793	0.6724	0.9475	1.9956	3.0153
10	1.0028	0.7122	0.3403	0.2265	0.9860	0.7224	0.4712	0.4807	0.6912	0.9732	2.0366	3.0608
11	1.0797	0.7650	0.3594	0.2359	1.0520	0.7272	0.4943	0.4773	0.6420	0.9061	1.9284	2.9382

3.4. X-rays Shielding Properties and Recommended Bi_2O_3 Contents of Three-Layered Bi_2O_3/NR Composites (Sample#4)

Figure 3 shows the values of the final I/I_0, μ_{eff}, $\mu_{m,eff}$, and HVL_{eff} of the three-layered Bi_2O_3/NR composites (sample#4, which provided higher X-ray shielding properties compared to the other designs), with varying Bi_2O_3 contents in layer#2 (middle layer) from 10 to 90 wt.% in 10 wt.% increments and a fixed combined thickness of 6 mm, determined at X-ray energies of 50, 100, 150, and 200 keV. The results indicated that the ability to attenuate incident X-rays greatly improved with increasing Bi_2O_3 contents, as evidenced by the decreases in the values of I/I_0 and HVL_{eff} and the increases in μ_{eff} and $\mu_{m,eff}$ with increasing contents. On the other hand, the overall shielding properties of the composites tended to decrease with increasing X-ray energy, as the lowest (highest) values of μ_{eff} and $\mu_{m,eff}$ (I/I_0 and HVL_{eff}) were observed at an X-ray energy of 200 keV. These two sets of behavior could be explained using Equation (12), which states that the photoelectric cross-section (σ_{pe}) (the ability to attenuate X-rays) is directly proportional to Z^n while being inversely proportional to ν^3 (E^3), resulting in enhanced (lower) shielding properties at higher filler contents (X-ray energies).

The $Pb_{eq,eff}$ values of the three-layered Bi_2O_3/NR composites (sample#4) with varying Bi_2O_3 contents in layer#2 (middle layer) from 10 to 90 wt.% in 10 wt.% increments and varying combined thicknesses of 6, 9, and 12 mm, are shown in Figure 4. The results indicated that the least Bi_2O_3 contents in layer#2, which could be regarded as the recommended Bi_2O_3 contents, that provided the three-layered NR composites with the required Pb_{eq} of 0.5 mmPb, were 82, 72, and 64 wt.% for the combined thicknesses of 6, 9, and 12 mm, respectively. The decreases in the recommended Bi_2O_3 contents with thicker samples were due to more Bi atoms being available in thicker materials (with the same filler content) to interact with incident X-rays, subsequently reducing the required Bi_2O_3 contents in layer#2. Notably, while it is possible to prepare NR composites with a 90 wt.% of fillers, as reported by Gwaily et al. who prepared Pb/NR composites for gamma shielding with the Pb contents up to 2000 phr (~95 wt.%) [31], difficulties in the sample preparation process, as well as possible substantial reductions in mechanical properties, could limit the processibility of multi-layered composites with very high filler contents. Consequently, for applications that allow space for thicker materials, lower recommended Bi_2O_3 fillers, such as those in 9 mm and 12 mm samples, should be considered to ease the difficulty and preserve the mechanical properties and product flexibility.

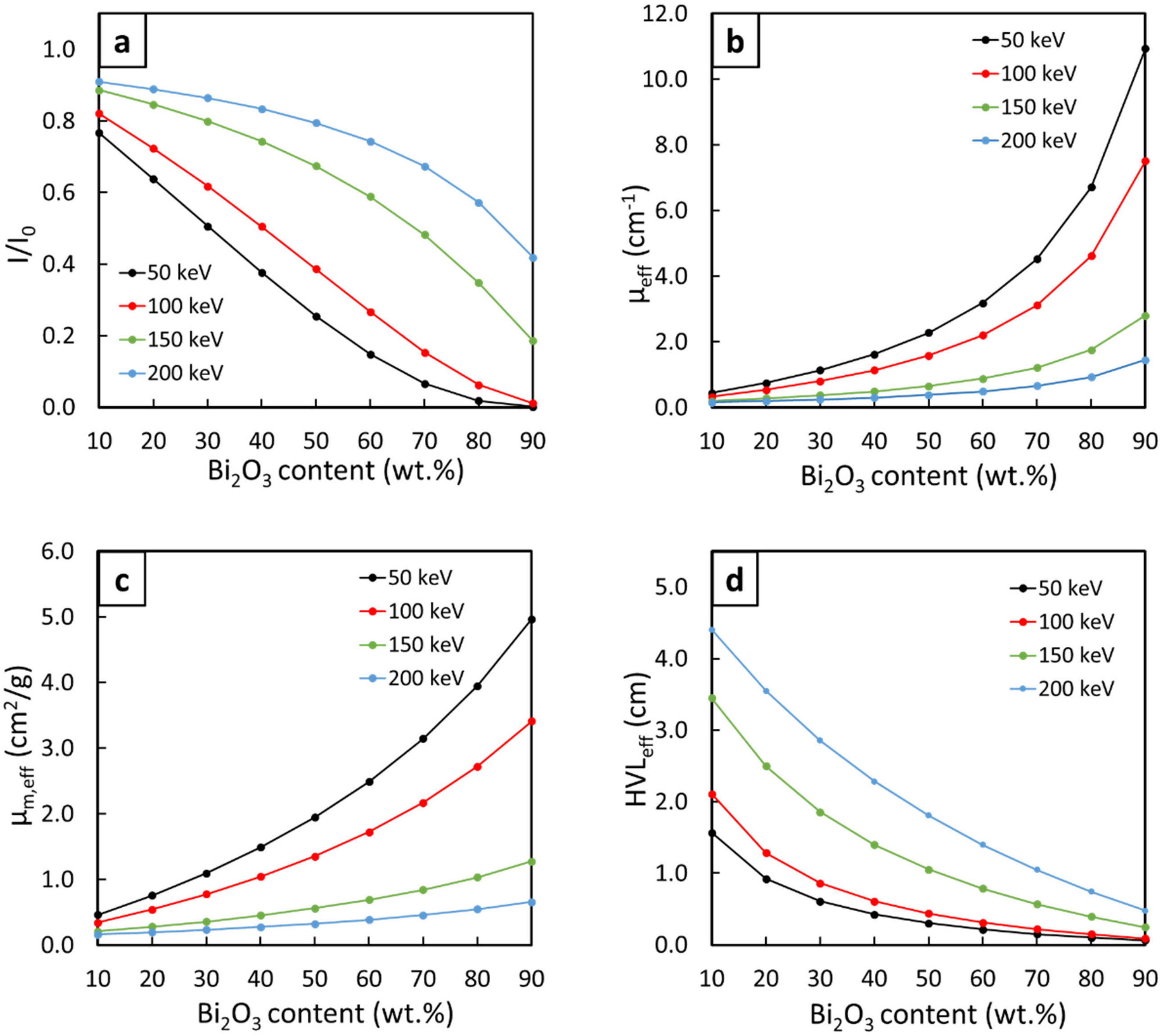

Figure 3. (**a**) Final values of I/I_0, (**b**) μ_{eff}, (**c**) $\mu_{m,eff}$, and (**d**) HVL_{eff} of three-layered Bi_2O_3/NR composites (sample#4) containing varying Bi_2O_3 contents from 10 to 90 wt.% in layer#2 (middle layer) and a fixed combined thickness of 6 mm, determined at X-ray energies of 50, 100, 150, and 200 keV.

In order to understand how the developed multi-layered structure (sample#4) performed with respect to previously reported materials, the results revealed that sample#4 in this work with the Bi_2O_3 content of 90 wt.% in layer#2 (middle layer) exhibited the μ value of 7.51 cm^{-1} (at 100 keV), while the dimensionally-enhanced wood/Bi_2O_3/NR composites and Gd_2O_3/NR composites with a total Bi_2O_3 content of 50 phr (approximately equal Bi_2O_3 content in the sample as those in sample#4) but with a single-layer structure, had the μ values of 2–3 and 2.6 cm^{-1} (at 100 keV), respectively [11,32]. These comparisons clearly indicate that the use of a multi-layered structure had great potential to substantially improve the X-ray shielding properties of the products.

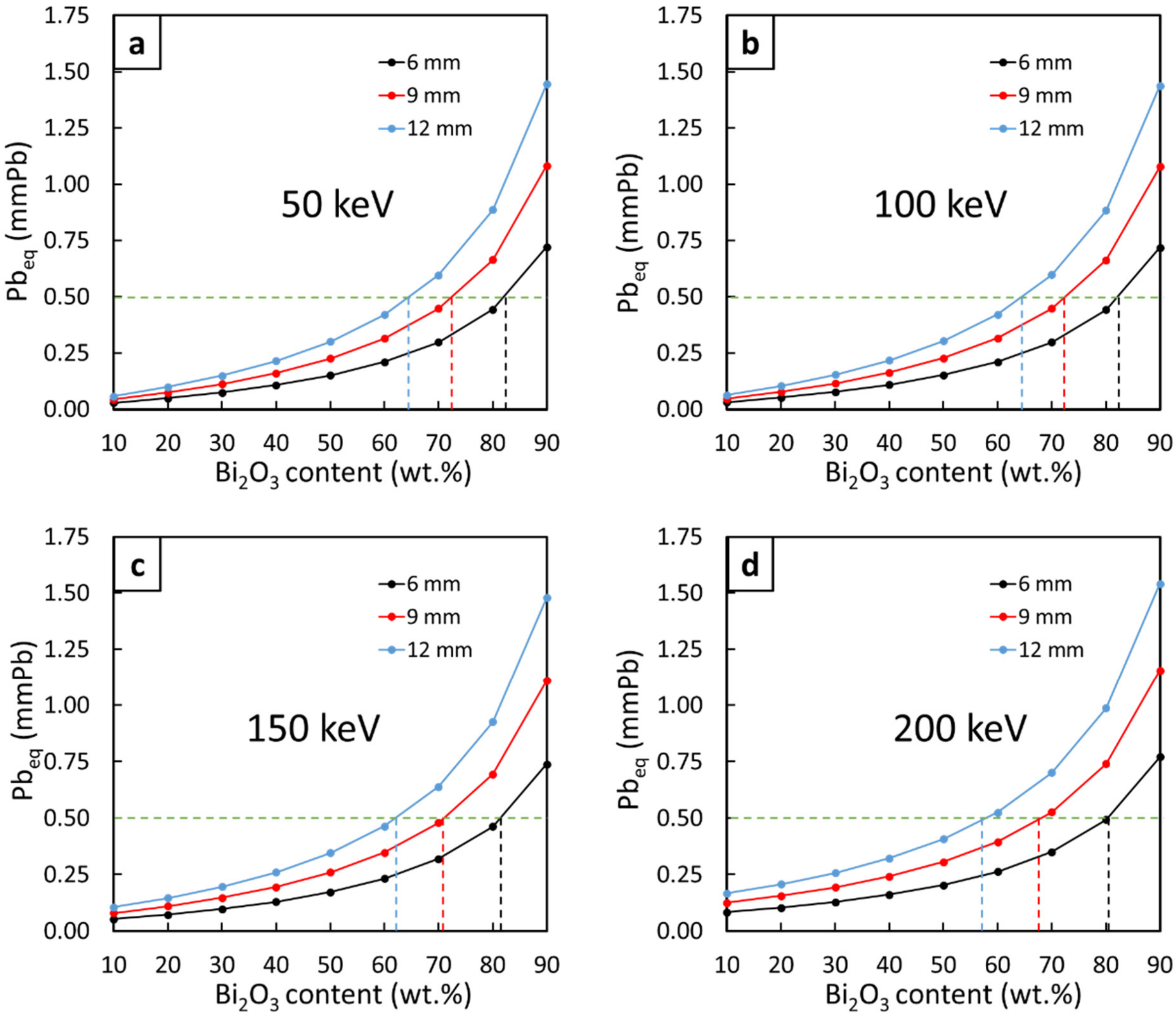

Figure 4. Effective Pb_{eq} of three-layered Bi_2O_3/NR composites (sample#4) with varying Bi_2O_3 contents from 10 to 90 wt.% in layer#2 (middle layer) and varying combined thicknesses of 6, 9, and 12 mm, determined at X-ray energies of (**a**) 50, (**b**) 100, (**c**) 150, and (**d**) 200 keV. The green dotted lines represent the common requirement of 0.5 mmPb used as a benchmark for this work and the blue, red, and black dotted lines represent the least Bi_2O_3 contents providing the composites with the Pb_{eq} of the required 0.5 mmPb for varying thicknesses.

4. Conclusions

This work theoretically compared the X-ray shielding properties of single-layered and multi-layered Bi_2O_3/NR composites by determining various shielding parameters (μ_{eff}, $\mu_{m,eff}$, HVL_{eff}, and $Pb_{eq,eff}$). In total, 11 different single-layered and multi-layered designs were used to investigate the X-ray attenuation capabilities at X-ray energies of 50, 100, 150, and 200 keV. The results indicated that the layers with higher Bi_2O_3 contents had better shielding abilities than those with lower contents and the three-layered structure (sample#4), with the layer arrangement of pristine NR (layer#1)-Bi_2O_3/NR (layer#2)-pristine NR (layer#3), had the highest overall X-ray shielding properties among the designs investigated, due to its highest effective Bi_2O_3 content, offering enhanced X-ray shielding properties of 10.5, 8.7, 4.0, and 2.1% compared to those of a single-layered structure (sample#1). Additionally, further investigation by varying the Bi_2O_3 contents in layer#2 (the middle layer) of sample#4 from 10 to 90 wt.% in 10 wt.% increments revealed that the X-ray shielding properties could be further enhanced by increasing the Bi_2O_3 contents; for which the recommended filler contents for actual production, determined from the common required Pb_{eq} value of 0.5 mm Pb, were 82, 72, and 64 wt.% for sample combined thicknesses of 6, 9, and

12 mm, respectively. The overall outcomes of this work reported not only the comparison of X-ray shielding properties of single-layered and multi-layered Bi_2O_3/NR composites but also presented potential methods to limit the reduction in mechanical properties and flexibility of the composites containing high filler contents.

Author Contributions: Conceptualization, K.S.; formal analysis, A.T., J.D. and K.S.; funding acquisition, K.S.; investigation, A.T., J.D. and K.S.; methodology, A.T., J.D. and K.S.; supervision, K.S.; validation, A.T., J.D. and K.S.; visualization, K.S.; writing—original draft, K.S.; writing—review and editing, A.T., J.D. and K.S. All authors have read and agreed to the published version of the manuscript.

Funding: This research was funded by the Kasetsart University Research and Development Institute (KURDI), Bangkok, Thailand, by grant number FF (KU)25.64.

Acknowledgments: The Kasetsart University Research and Development Institute (KURDI) and the Specialized Center of Rubber and Polymer Materials in Agriculture and Industry (RPM) provided publication support.

Conflicts of Interest: The authors declare no conflict of interest. The funders had no role in the design of the study; in the collection, analyses, or interpretation of data; in the writing of the manuscript, or in the decision to publish the results.

References

1. Cole, L.E.; Ross, R.D.; Tilley, J.M.R.; Vargo-Gogola, T.; Roeder, R.K. Gold nanoparticles as contrast agents in X-ray imaging and computed tomography. *Nanomedicine* **2015**, *10*, 321–341. [CrossRef] [PubMed]
2. Miao, J.; Ishikawa, T.; Robinson, I.K.; Murnane, M.M. Beyond crystallography: Diffractive imaging using coherent x-ray light sources. *Science* **2015**, *348*, 530–535. [CrossRef] [PubMed]
3. Rogers, T.W.; Jaccard, N.; Morton, E.J.; Griffin, L.D. Automated X-ray image analysis for cargo security: Critical review and future promise. *J. X-ray Sci. Technol.* **2017**, *25*, 33–56. [CrossRef] [PubMed]
4. Mayo, S.C.; Stevenson, A.W.; Wilkins, S.W. In-line phase-contrast X-ray imaging and tomography for materials science. *Materials* **2012**, *5*, 937–965. [CrossRef]
5. Cotte, M.; Susini, J.; Dik, J.; Janssens, K. Synchrotron-based X-ray absorption spectroscopy for art conservation: Looking back and looking forward. *Acc. Chem. Res.* **2010**, *43*, 705–714. [CrossRef]
6. Scholz, A.M.; Bunger, L.; Kongsro, J.; Baulain, U.; Mitchell, A.D. Non-invasive methods for the determination of body and carcass composition in livestock: Dual-energy X-ray absorptiometry, computed tomography, magnetic resonance imaging and ultrasound: Invited review. *Animal* **2015**, *9*, 1250–1264. [CrossRef]
7. Poltabtim, W.; Wimolmala, E.; Markpin, T.; Sombatsompop, N.; Rosarpitak, V.; Saenboonruang, K. X-ray shielding, mechanical, physical, and water absorption properties of wood/PVC composites containing bismuth oxide. *Polymers* **2021**, *13*, 2212. [CrossRef]
8. Balonov, M.I.; Shrimpton, P.C. Effective dose and risks from medical x-ray procedures. *Ann. ICRP* **2012**, *41*, 129–141. [CrossRef]
9. Bevelacqua, J.J. Practical and effective ALARA. *Health Phys.* **2010**, *98*, S39–S47. [CrossRef]
10. Toyen, D.; Paopun, Y.; Changjan, D.; Wimolmala, E.; Mahathenabodee, S.; Pianpanit, T.; Anekratmontree, T.; Saenboonruang, K. Simulation of neutron/self-emitted gamma attenuation and effects of silane surface treatment on mechanical and wear resistance properties of Sm_2O_3/UHMWPE composites. *Polymers* **2021**, *13*, 3390. [CrossRef]
11. Saenboonruang, K.; Poltabtim, W.; Thumwong, A.; Pianpanit, T.; Rattanapongs, C. Rare-earth oxides as alternative high-energy photon protective fillers in HDPE composites: Theoretical aspects. *Polymers* **2021**, *13*, 1930. [CrossRef] [PubMed]
12. Alsayed, Z.; Badawi, M.S.; Awad, R.; Thabet, A.A.; El-Khatib, A.M. Study of some γ-ray attenuation parameters for new shielding materials composed of nano ZnO blended with high density polyethylene. *Nucl. Technol. Radiat. Prot.* **2019**, *34*, 342–352. [CrossRef]
13. Toyen, D.; Rittirong, A.; Poltabtim, W.; Saenboonruang, K. Flexible, lead-free, gamma-shielding materials based on natural rubber/metal oxide composites. *Iran. Polym. J.* **2018**, *27*, 33–41. [CrossRef]
14. Poltabtim, W.; Wimolmala, E.; Saenboonruang, K. Properties of lead-free gamma-ray shielding materials from metal oxide/EPDM rubber composites. *Radiat. Phys. Chem.* **2018**, *153*, 1–9. [CrossRef]
15. Cherkasov, V.; Yurkin, Y.; Avdonin, V.; Suntsov, D. Self-adhesion X-ray shielding composite material of EPDM rubber with barite: Mechanical properties. *Mater. Plast.* **2020**, *57*, 26–36. [CrossRef]
16. Dejangah, M.; Ghojavand, M.; Pourselehi, R.; Gholipour, P.R. X-ray attenuation and mechanical properties of tungsten-silicone rubber nanocomposites. *Mater. Res. Express* **2019**, *6*, 085045. [CrossRef]
17. Yu, L.; Yap, P.L.; Santos, A.; Tran, D.; Losic, D. Lightweight bismuth titanate ($Bi_4Ti_3O_{12}$) nanoparticle-epoxy composite for advanced lead-free X-ray radiation shielding. *ACS Appl. Nano Mater.* **2021**, *4*, 7471–7478. [CrossRef]
18. Mason, L.H.; Harp, J.P.; Han, D.Y. Pb neurotoxicity: Neuropsychological effects of lead toxicity. *BioMed Res. Int.* **2014**, *2014*, 840547. [CrossRef]

19. Sayyed, M.I.; Almuqrin, A.H.; Kurtulus, R.; Javier-Hila, A.M.V.; Kaky, K.; Kavas, T. X-ray shielding characteristics of P_2O_5–Nb_2O_5 glass doped with Bi_2O_3 by using EPICS2017 and Phy-X/PSD. *Appl. Phys. A* **2021**, *127*, 243. [CrossRef]
20. Intom, S.; Kalkornsurapranee, E.; Johns, J.; Kaewjaeng, S.; Kothan, S.; Hongtong, W.; Chaiphaksa, W.; Kaewkhao, J. Mechanical and radiation shielding properties of flexible material based on natural rubber/Bi_2O_3 composites. *Radiat. Phys. Chem.* **2020**, *172*, 108772. [CrossRef]
21. Brechet, Y.; Cavaille, J.Y.; Chabert, E.; Chazeau, L.; Dendievel, R.; Flandin, L.; Gauthier, C. Polymer based nanocomposites: Effect of filler-filler and filler-matrix interactions. *Adv. Eng. Mater.* **2001**, *3*, 571–577. [CrossRef]
22. Jiang, X.; Yang, Z.; Wang, Z.; Zhang, F.; You, F.; Yao, C. Preparation and sound absorption properties of a barium titanate/nitrile butadiene rubber-polyurethane foam composite with multilayered structure. *Materials* **2018**, *11*, 474. [CrossRef] [PubMed]
23. VIGO. Multilayer Rubber Pad. Available online: https://www.vigohvac.com/multilayer-rubber-pad/ (accessed on 23 March 2022).
24. Bagheri, R.; Maghaddam, A.K.; Yousefnia, H. Gamma Ray Shielding Study of Barium–Bismuth–Borosilicate Glasses as Transparent Shielding Materials using MCNP-4C Code, XCOM Program, and Available Experimental Data. *Nucl. Eng. Technol.* **2017**, *49*, 216–223. [CrossRef]
25. Berger, M.J.; Hubbell, J.H.; Seltzer, S.M.; Chang, J.; Coursey, J.S.; Sukumar, R.; Zucker, D.S.; Olsen, K. *XCOM: Photon Cross Section Database (Version 1.5)*; National Institute of Standards and Technology: Gaithersburg, MD, USA, 2010. Available online: http://physics.nist.gov/xcom (accessed on 30 January 2021).
26. Livet, F.; Sutton, M. X-ray coherent scattering in metal physics. *C. R. Phys.* **2012**, *13*, 227–236. [CrossRef]
27. Sato, T.; Iwamoto, Y.; Hashimoto, S.; Ogawa, T.; Furuta, T.; Abe, S.; Kai, T.; Tsai, P.E.; Matsuda, N.; Iwase, H.; et al. Features of particle and heavy ion transport code system PHITS version 3.02. *J. Nucl. Sci. Technol.* **2018**, *55*, 684–690. [CrossRef]
28. Shik, N.A.; Gholamzadeh, L. X-ray shielding performance of the EPVC composites with micro- or nanoparticles of WO_3, PbO or Bi_2O_3. *Appl. Radiat. Isot.* **2018**, *139*, 61–65. [CrossRef]
29. Al-Arif, M.S.; Kakil, D.O. Calculated-Experimental Model for Multilayer Shield. *ARO Sci. J. Koya Univ.* **2015**, *3*, 10057.
30. Akyildirim, H.; Waheed, F.; Gunoglu, K.; Akkurt, I. Investigation of buildup factor in gamma-ray measurement. *Act. Phys. Pol.* **2017**, *132*, 1203–1206. [CrossRef]
31. Gwaily, S.E.; Madani, M.; Hassan, H.H. Lead-Natural rubber composites as gamma radiation shields. II: High concentration. *Polym. Compos.* **2002**, *23*, 495–499. [CrossRef]
32. Poltabtim, W.; Toyen, D.; Saenboonruang, K. Theoretical Determination of high-energy photon attenuation and recommended protective filler contents for flexible and enhanced dimensionally stable wood/NR and NR composites. *Polymers* **2021**, *13*, 869. [CrossRef]